NIH Public Access
Author Manuscript
Neuron. Author manuscript; available in PMC 2012 April 6.

Published in final edited form as:
Neuron. 2011 October 6; 72(1): 49–56. doi:10.1016/j.neuron.2011.08.020.

Recurrent circuitry dynamically shapes the activation of piriform cortex

Kevin M. Franks[1,4], **Marco J. Russo**[1,4], **Dara L. Sosulski**[1,4], **Abigail A. Mulligan**[3,4], **Steven A. Siegelbaum**[1,2,4], and **Richard Axel**[1,3,4]

[1]Department of Neuroscience, College of Physicians and Surgeons, Columbia University, New York, New York 10032, USA

[2]Department of Pharmacology College of Physicians and Surgeons, Columbia University, New York, New York 10032, USA

[3]Department of Biochemistry and Molecular Biophysics College of Physicians and Surgeons, Columbia University, New York, New York 10032, USA

[4]Howard Hughes Medical Institute, College of Physicians and Surgeons, Columbia University, New York, New York 10032, USA

Summary

In the piriform cortex, individual odorants activate a unique ensemble of neurons that are distributed without discernable spatial order. Piriform neurons receive convergent excitatory inputs from random collections of olfactory bulb glomeruli. Pyramidal cells also make extensive recurrent connections with other excitatory and inhibitory neurons. We have introduced channelrhodopsin into piriform cortex to characterize these intrinsic circuits and examine their contribution to activity driven by afferent bulbar inputs. We demonstrate that individual pyramidal cells are sparsely interconnected by thousands of excitatory synaptic connections that extend, largely undiminished, across piriform cortex, forming a large excitatory network that can dominate the bulbar input. Pyramidal cells also activate inhibitory interneurons that mediate strong, local feedback inhibition that scales with excitation. This recurrent network can enhance or suppress bulbar input, depending on whether the input arrives before or after the cortex is activated. This circuitry may shape the ensembles of piriform cells that encode odorant identity.

Introduction

Sensory information is transmitted to the brain where it is processed to create an internal representation of the external world. In vision and touch, information central to perception is ordered in space in the external world and this order is maintained from the peripheral sense organs to the cortex. The quality of an odor, however, does not exhibit a discernible spatial order in the physical world and this poses the question of how odors are represented in the brain. Olfactory perception is initiated by the recognition of odorant molecules by a large repertoire of receptors in the olfactory sensory epithelium (Buck and Axel, 1991). Individual olfactory neurons express one of approximately 1,000 receptors and each receptor interacts

© 2011 Elsevier Inc. All rights reserved

Correspondence: Richard Axel 701 W. 168th St, HHSC, 1014, New York, NY, 10032 ra27@columbia.edu (212) 305-6915.

Publisher's Disclaimer: This is a PDF file of an unedited manuscript that has been accepted for publication. As a service to our customers we are providing this early version of the manuscript. The manuscript will undergo copyediting, typesetting, and review of the resulting proof before it is published in its final citable form. Please note that during the production process errors may be discovered which could affect the content, and all legal disclaimers that apply to the journal pertain.

NIH-PA Author Manuscript
NIH-PA Author Manuscript
NIH-PA Author Manuscript

NIH-PA Author Manuscript

NIH-PA Author Manuscript

NIH-PA Author Manuscript

with multiple odorants (Chess et al., 1994; Malnic et al., 1999). Neurons expressing a given receptor project with precision to two spatially invariant glomeruli in the olfactory bulb (Mombaerts et al., 1996). Thus, the randomly distributed population of neurons activated by an odorant in the olfactory epithelium is consolidated into a discrete, stereotyped map of glomerular activity in the olfactory bulb (Bozza et al., 2004; Meister and Bonhoeffer, 2001; Rubin and Katz, 1999; Uchida et al., 2000).

This highly ordered map of spatially invariant glomeruli must then be integrated and transformed in higher olfactory centers to encode the synthetic features of odors. Mitral and tufted cells each extend an apical dendrite into a single glomerulus, and send axons to several telencephalic areas, including significant input to the piriform cortex. Anatomic tracing reveals that axons from individual glomeruli project diffusely to the piriform without apparent spatial order (Ghosh et al., 2011; Miyamichi et al., 2011; Sosulski et al., 2011). Electrophysiological (Poo and Isaacson, 2009) and optical imaging (Stettler and Axel, 2009) experiments reveal that individual odorants activate sparse subpopulations of neurons distributed across the piriform without spatial preference. These data are in accord with a model in which piriform neurons receive convergent input from random collections of glomeruli (Davison and Ehlers, 2011; Stettler and Axel, 2009). The piriform therefore discards the spatial segregation of the bulb and returns to a highly dispersed organization in which different odorants activate unique ensembles of cortical neurons.

Piriform neurons are intricately connected through a network of recurrent excitatory and inhibitory synapses (Haberly and Price, 1978; Johnson et al., 2000b; Ketchum and Haberly, 1993; Luskin and Price, 1983a, b; Price, 1973; Stevens, 1969) that may shape the olfactory representation to accommodate the computational requirements that underlie olfactory perception. These include gain control, pattern separation, and pattern completion, as well as odor learning (Haberly, 2001; Haberly and Bower, 1989; Linster and Hasselmo, 2001; Saar et al., 2002; Wilson and Stevenson, 2003). We have introduced channelrhodopsin (ChR2; Boyden et al., 2005; Nagel et al., 2003) into piriform cortex to characterize these intrinsic circuits and examine their contribution to pyramidal cell activity driven by afferent bulbar inputs in mouse brain slices. We find that pyramidal cell axons project across piriform cortex, but make excitatory synaptic contacts with less than 1% of other pyramidal cells. However, the large number of cells in piriform ensures that each cell receives inputs from at least 2000 other pyramidal cells. Pyramidal cells also activate inhibitory interneurons that mediate strong, local feedback inhibition that scales with excitation. We demonstrate that this recurrent network dynamically boosts or inhibits the spiking of pyramidal cells in response to bulbar inputs, depending on the relative timing of the two sets of inputs, suggesting that recurrent piriform circuitry can shape the ensembles of odor-responsive neurons in piriform cortex.

Results

We expressed high levels of channelrhodopsin-2 (ChR2) in a focal subpopulation of neurons in anterior piriform cortex by an intersectional infection with two viruses. Adeno-associated virus (AAV) encoding Cre-dependent ChR2-YFP was co-injected with lentivirus encoding Cre recombinase (Figure 1A). This strategy ensures high ChR2 expression that is limited by the spread of the lentiviral vector to a focal subset of excitatory and inhibitory neurons. Cre-positive, ChR2-expressing neurons were largely restricted to a focal cluster of layer II/III cells a few hundred microns wide (Figure 1Bi), although axons of YFP-expressing cells were observed throughout the rostrocaudal extent of the piriform (Figure 1Bii).

We prepared acute parasagittal brain slices through piriform cortex from 8–12 week-old mice. Typically, one slice per animal included a significant extent of piriform cortex along

NIH-PA Author Manuscript

NIH-PA Author Manuscript

NIH-PA Author Manuscript

the rostrocaudal axis containing a focal area of YFP fluorescence (Figure 1C). Whole-cell recordings were then obtained from multiple layer II pyramidal cells (Figure S1A–C) at different distances from the center of the infection site. A 500-ms light pulse centered on the somata of cells at the site of infection evoked robust and sustained photocurrents in a subset of these cells (Figure 1D, S1D). At the center of the fluorescence cloud, 35% of neurons were ChR2-positive ($ChR2^+$, defined by the presence of a sustained photocurrent) but the frequency of $ChR2^+$ cells diminished dramatically with distance from the center of the infected area. In contrast, the magnitude of the photocurrent in $ChR2^+$ cells did not decrease with distance from the injection site (Figure 1E).

We next determined the connectivity of this focal set of $ChR2^+$ cells with ChR2-negative ($ChR2^-$) pyramidal cells across the piriform. A light pulse focused on $ChR2^-$ cells distant from the site of infection elicited transient inward currents in voltage-clamp recordings at −70 mV. These currents were blocked by AMPA and NMDA receptor antagonists, indicating that these were excitatory postsynaptic currents (EPSCs) evoked from the axons of $ChR2^+$ neurons (Figure 1F). These light-evoked synaptic responses exhibited properties consistent with those described for “associational” piriform synapses (Franks and Isaacson, 2005; Figure S2A–C). Monosynaptic (Figure S2D, E), light-evoked EPSCs were observed in 94 of 95 recorded $ChR2^-$ cells across the piriform in slices from 11 animals (Figure 1G). Interestingly, the EPSC amplitude was largely independent of the distance of the recorded cell from the infection site (Figure 1H, J). These data indicate that extend, undiminished, across millimeters of piriform cortex. This pattern of long-range excitatory connectivity in piriform was also apparent when a modified rabies virus was used as retrograde tracer (Wickersham et al., 2007) to map the cells that provide synaptic input to pyramidal cells (Figure S2F–I).

The long-range excitatory recurrent projections in piriform contrasts with the pattern of connectivity we observed upon focal expression of ChR2 in primary somatosensory (S1) and visual (V1) cortex. In both S1 and V1 (not shown), there was a steep decrease in light-evoked EPSC amplitude in layer II/III pyramidal neurons with increasing distance from the infection center (Figure 1I, J). Thus, unlike neurons in S1 and V1 that preferentially connect to more proximal targets, a given piriform neuron forms synapses onto layer II pyramidal cells with similar probability across the cortex.

We next obtained a quantitative estimate of the number and strength of the intrinsic excitatory inputs onto a given piriform neuron. The amplitudes of the light-evoked EPSCs were large, but somewhat variable within a given animal (mean ± S.D.: 441 ± 334 pA; C.V., 0.76; n=95 cells from the 11 animals/slices, Figure 2A). These large EPSCs were presumably mediated by inputs from many $ChR2^+$ axons, each of which contributes a unitary response (uEPSC). To determine the number of $ChR2^+$ axonal inputs underlying the light-evoked response we first determined the strength of a single recurrent input. We decreased the intensity and field of illumination of the light pulse to achieve threshold activation of a single $ChR2^+$ axonal input, which was indicated by interleaved successful responses and failures to these light pulses (Figure 2B). The mean size of the uEPSC was 36.2 pA (± 20.3 pA, S.D.; range: 16–74 pA, n=10), though our measurements may be biased towards slightly larger, more easily resolved responses. The success rate (0.52 ± 0.047; n=10) places a lower bound on the probability of synaptic vesicle release at recurrent synapses.

We next determined the number of synaptic contacts each $ChR2^+$ axon makes onto a given layer II pyramidal cell by measuring quantal responses (qEPSC) evoked by replacing extracellular Ca^{2+} with Sr^{2+} to desynchronize synaptic release. In slices bathed in Sr^{2+}, light pulses evoked a large, early synchronous response with a tail of many small events that are

NIH-PA Author Manuscript

NIH-PA Author Manuscript

NIH-PA Author Manuscript

thought to represent quantal synaptic currents (Dodge et al., 1969; Franks and Isaacson, 2006; Goda and Stevens, 1994; Figure 2Ci). The similar amplitude of the light-evoked uEPSCs and qEPSCs (25 pA ± 10 pA, S.D.; n=11; Figure 2Cii, iv) suggests that a recurrent axon typically makes single, en passant synaptic contacts with a given pyramidal cell in piriform cortex, consistent with anatomical predictions (Datiche et al., 1996; Johnson et al., 2000a). Moreover, at this contact, a presynaptic action potential releases, at most, a single quantum of transmitter. The light-evoked qEPSCs were larger and had faster kinetics than qEPSCs evoked from electrical stimulation of mitral and tufted cell axons in the lateral olfactory tract (LOT) in the same cells (14 pA ± 4.0 pA, n=9, Figure 2Ciii, iv). The amplitudes of qEPSCs from afferent and recurrent inputs are consistent with the range of amplitudes of miniature EPSCs we recorded in TTX (17.3 ± 7.1 pA, S.D.; n = 562 events, 9 cells). The difference in the size of the afferent and recurrent qEPSCs may reflect differences in their biophysical properties (Schikorski and Stevens, 1999) or may simply reflect greater dendritic filtering of the more distal LOT inputs.

The ratio between the average EPSC (500 pA) evoked with a saturating light intensity that activates all $ChR2^+$ inputs (see Figure 3F) and the unitary ESPC (25 pA) suggests that a cell receives, on average, 20 active inputs from the population of $ChR2^+$ neurons. From the distribution of $ChR2^+$ cells, we estimate that we infected about 8000 excitatory neurons per animal (Figure S1E–H). This implies that the connectivity between any two pyramidal cells is less than 1%, and this value is largely independent of the distance between two piriform cells. Moreover, given that we infected less than 1% of all piriform pyramidal neurons (8000 neurons out of a total of an assumed 10^6 pyramidal cells in the piriform), our observation of 20 activated $ChR2^+$ inputs per cell implies that that each neuron receives, at least, 2000 recurrent excitatory inputs. In contrast, pyramidal cells are thought to receive only about 200 afferent inputs from the bulb (Davison and Ehlers, 2011). These inputs, however, are multiquantal and can be quite large, with each axon typically making ~5 contacts per cell (Bathellier et al., 2009; Franks and Isaacson, 2006); but see (McGinley and Westbrook, 2011; Suzuki and Bekkers, 2011). Individual pyramidal cells may therefore receive strong inputs from 200 mitral/tufted cells in the bulb and weak inputs from more than 2000 pyramidal cells across piriform cortex.

This recurrent network would result in runaway excitation in response to odor unless its activity was tempered by inhibition. To investigate the role of inhibition in modulating the activity of the recurrent excitatory network, we isolated the inhibitory synaptic current by recording from pyramidal cells at a voltage near the equilibrium potential for EPSCs (V_m = +5 mV). We first recorded from $ChR2^-$ cells close to the infection site in the presence of NBQX and APV to block glutamatergic transmission. Under these conditions, light pulses evoked outward currents that were blocked by the $GABA_A$-receptor antagonist gabazine (GBZ, Figure 3Ai), indicating that these were inhibitory postsynaptic currents (IPSCs) originating directly from $ChR2^+$ GABAergic neurons. Although all cells in or near the infection site showed direct IPSCs, direct inhibition rapidly decayed at distances >300 μm beyond the edge of the infected area, indicating that this direct inhibition is local (Figure 3B).

In contrast to the local direct inhibition, when inhibitory currents were recorded with excitatory transmission intact, we observed large IPSCs in almost every neuron, regardless of distance from the site of infection (85/87 cells; Figure 3Aii,B). Because direct inhibition is local, inhibitory currents distant from the site of infection must result from the activation of long-range excitatory $ChR2^+$ axons that synaptically activate local inhibitory interneurons. The long-range inhibitory responses lagged behind the onset of the light-evoked EPSCs recorded in the same cells by 1.6 ± 0.12 ms (n=21) and were abolished by NBQX and APV (Figure 3Aii), indicating that this inhibition was disynaptic and driven by

NIH-PA Author Manuscript

NIH-PA Author Manuscript

NIH-PA Author Manuscript

axons of $ChR2^+$ excitatory cells. Our methodology therefore allows us to selectively isolate disynaptic inhibition by recording from cells far from the infection site where the light-evoked IPSC is not contaminated by direct inputs from $ChR2^+$ inhibitory neurons.

A comparison of the magnitudes of the excitatory and disynaptic inhibitory currents in a given cell revealed that the inhibitory response was much larger than the excitatory response (Figure 3C). We compared the input-output relationship of excitation versus inhibition by recording the excitatory and inhibitory responses to a series of light pulses of increasing intensity (Figure 3D). Increasing the intensity of the light pulse increased the excitatory responses from a level at which we failed to observe any synaptic response to a level at which the EPSC amplitudes saturated and failed to increase with increasing light intensity. The IPSC scaled with, and dominated, the EPSC across the entire range of stimulus intensities (Figure 3E). We also determined the laminar organization of the recurrent excitatory and inhibitory synaptic inputs onto layer II pyramidal cells using focal illumination along the cell's apical-basal axis in the presence of TTX/4-AP (Petreanu et al., 2009). These experiments indicate that pyramidal cells receive the majority of their recurrent excitatory input onto their proximal apical dendrites in layer Ib, whereas feedback inhibition is preferentially recruited by their axons projecting through layer III (Figure S3).

How do these recurrent circuits shape the response of piriform neurons to bulbar inputs? We paired a brief train of electrical LOT stimuli that mimics the burst firing of a mitral cell to odorant stimulation (Cang and Isaacson, 2003; Margrie and Schaefer, 2003) with a brief train of light pulses in piriform cortex (both stimuli, 5 pulses at 40 Hz; i.e. a 100 ms burst) and recorded the responses in pyramidal cells in current clamp. The stimulus strengths were adjusted to evoke spiking in 10% of the trials when either stimulus was presented alone (probability of spiking was 0.10 ± 0.38 following electrical stimulation of the LOT and was 0. 10 ± 0.054 with light-activation of piriform; n=6). In contrast to the low probability of spiking when LOT or piriform was activated alone, action potentials were evoked in 90% of the trials (0.90 ± 0.056) when the two inputs were presented simultaneously (Figure 4A).

We next examined the effect of altering the temporal relationship between the pairing of bulbar and recurrent inputs. No increase in spiking was observed when the onset of the two 100 ms-long bursts of stimuli were 150 ms apart. However, when the LOT train was delivered 100 ms before the piriform train, such that the last LOT-evoked input coincided with the first light-evoked input, the cell fired action potentials in 75% of the trials (0.75 ± 0.098; Figure 4B,C). In contrast, no enhancement in spike firing was observed when the piriform train arrived 100 ms before the LOT input (0.20 ± 0.073; unpaired t-test vs. LOT alone, p=0.423; vs. PCx alone, p=0.315; Figure 4B,C).

We then examined the role of inhibition in this pairing paradigm by repeating these experiments in the presence of GBZ and the $GABA_B$ antagonist, CGP55845. Blocking inhibition broadened the time window over which spiking could be enhanced by pairing the inputs (Figure 4C). Furthermore, the efficacy with which the pairing of the inputs enhanced the response was less dependent on the order in which the two inputs were presented (skewness of control distribution, 0.64 ± 0.17, n=6; skewness of distribution in GBZ, 0.21 ± 0.04, n=4; unpaired t-test, $p < 0.05$). This result implies that much of the asymmetry we observed in the efficacy of pairing order is a consequence of inhibition.

We hypothesized that the response to LOT inputs might be suppressed by prior activation of the cortical circuitry because of the recruitment of strong feedback inhibition. This prediction was tested by delivering a short train of LOT stimulation (3 pulses at 40 Hz) to achieve spiking on half the trials (0.56 ± 0.042). Indeed, when a similar train of piriform stimuli (3 pulses at 40 Hz; probability of spiking; 0.36 ± 0.16) preceded the LOT input by

NIH-PA Author Manuscript

NIH-PA Author Manuscript

NIH-PA Author Manuscript

100 ms, we observed an 18% reduction in the probability of spiking. (LOT train following PCx train, 0.46 ± 0.049; n=9 cells; paired t-test comparing two LOT trains, p = 0.017; Figure 4D).

Two forms of inhibition have been described in the piriform cortex. Feedforward inhibition is mediated by interneurons in layer I that receive direct input from the LOT and synapse on apical dendrites of pyramidal cells, whereas feedback inhibition is mediated by the layer II/III interneurons that are activated by pyramidal cells and synapse onto pyramidal cell bodies (Luna and Schoppa, 2008; Neville and Haberly, 2004; Stokes and Isaacson, 2010; Suzuki and Bekkers, 2010). Two experimental approaches were employed to demonstrate that feedback inhibition is significantly stronger than feedforward inhibition. We observed a dramatically greater effect of gabazine on synaptic responses following subthreshold recurrent stimulation versus LOT stimulation (Figure S4A). We also determined the lowest stimulation intensities of either the LOT or recurrent inputs that reliably drove spiking when inhibition was blocked. LOT stimulation at this intensity could still generate spiking when inhibition was intact (Figure S4), consistent with a relatively small role for feedforward inhibition. In contrast, piriform stimulation at this intensity always failed to evoke spikes in downstream piriform neurons when inhibition was intact. These data support a dominant role for feedback versus feedforward inhibition in controlling the activation of piriform cortex pyramidal cells.

Discussion

In piriform cortex, the specificity of an odorant is represented by a unique ensemble of neurons that is distributed without discernable spatial order. These cells also make extensive recurrent connections with other excitatory and inhibitory neurons that may shape the odorant representation. We have introduced ChR2 into focal regions of piriform cortex to study the role of recurrent circuitry in shaping the cortical response to bulbar input. Axons of layer II/III pyramidal cells project across piriform cortex where they make excitatory synaptic contacts with other pyramidal cells. The likelihood that any two pyramidal cells are synaptically connected is very small, but remains roughly constant over remarkably long distances compared to neocortical sensory areas. However, as a consequence of the large number of piriform cells, each cortical neuron receives excitatory inputs from at least 2000 other pyramidal cells. Pyramidal cells also activate GABAergic interneurons that form powerful inhibitory synapses onto nearby pyramidal cells to counter, and often overwhelm, the recurrent excitation. The recurrent circuitry in piriform cortex therefore produces global excitation that recruits strong local inhibition, which scales with the excitatory drive. This allows temporal pairing of bulbar input with activation of the recurrent network to alter piriform responses, thereby shaping the odor representation.

Projections from individual glomeruli are distributed throughout piriform cortex without any obvious topographic order, and individual pyramidal cells receive convergent input from a random collection of glomeruli. This afferent information is then redistributed across piriform by the diffuse and apparently random recurrent network. Nevertheless, an odor will consistently activate the same ensemble of piriform neurons in an individual (Poo and Isaacson, 2009; Stettler and Axel, 2009).

We consider two distinct models for the activation of a cortical odor ensemble. In one model, an odorant may activate a sufficient number of mitral and tufted cell inputs to generate a direct, suprathreshold synaptic response in all of the odor-responsive piriform neurons. In this case, the long-range recurrent excitation would mainly serve to recruit inhibitory neurons to generate a strong, diffuse feedback inhibition. Alternatively, an odorant may evoke suprathreshold input from the olfactory bulb in a small subset of odor-

NIH-PA Author Manuscript

NIH-PA Author Manuscript

NIH-PA Author Manuscript

responsive neurons. This small fraction of spiking piriform cells would then generate sufficient recurrent excitation to recruit a larger population of neurons that receive subthreshold afferent input. The strong feedback inhibition resulting from activation of this larger population of neurons would then suppress further spiking and prevent runaway recurrent excitation. In the extreme, some cells could receive enough recurrent input to fire action potentials without receiving afferent input.

Two recent studies lend support to the second model. First, Davison and Ehlers (2011) observed robust responses in piriform neurons upon activation of a set of glomeruli were not synaptically connected to the recorded cell. Second, Poo and Isaacson (2011) observe that, in a subpopulation of cells, afferent, LOT input only accounts for a small fraction of the odor-evoked excitatory drive onto a layer II pyramidal cells. Our studies demonstrate that pairing weak bulbar inputs with recurrent inputs can dramatically increase the activation of piriform neurons. These effects are observed even though we expressed ChR2 in less than 1% of piriform neurons. Thus the spiking of only a small fraction of piriform cells by direct input from the bulb could activate the recurrent circuitry to recruit the ensemble of odor-responsive neurons. Recurrent input could therefore contribute significantly to the activation of a piriform ensemble, though these data do not exclude models in which piriform pyramidal cells are driven largely by bulbar input.

Our results indicate that the effect of recurrent input on the ability of olfactory bulb input to drive spiking is highly dependent on the relative timing of the two sets of inputs. When piriform axons are activated simultaneously with or slightly after stimulation of the LOT, the firing of piriform neurons is significantly enhanced. However, when piriform is activated prior to stimulation of the LOT, the firing of piriform neurons in response to LOT inputs is suppressed. This dynamic circuitry is poised to generate a homogenous, associative network that can potentially explain a number of features of olfactory processing observed in piriform. For example, the number of odor-responsive neurons in piriform is only weakly dependent on odorant concentration (Stettler and Axel, 2009), even though both the number of activated glomeruli (Rubin and Katz, 1999) and the amount of excitatory input to individual piriform pyramidal cells (Poo and Isaacson, 2009) increases with odorant concentration. A diffuse recurrent cortical network with scaled inhibition affords a normalization mechanism that can maintain a constant level of piriform activation. The recurrent piriform network may also explain the observation that the number of piriform neurons activated by a mixture of odorants is far less than the sum of the neurons activated by individual odorant components. Rather, odorant mixtures tend to suppress activity in cells responsive to individual odorants presented alone (Stettler and Axel, 2009). Thus, the pattern of active neurons in response to a mixture of odorants differs from the representation of individual components. A highly interconnected recurrent network might accommodate these computations (Barkai et al., 1994; Haberly, 2001; Haberly and Bower, 1989; Wilson and Bower, 1992).

We find that the recurrent circuitry in piriform cortex exhibits organizational properties that are different from those of sensory neocortices. In vision, touch and hearing, spatial information in the peripheral sense organ is maintained in the cortex. In sensory neocortex, cells responsive to similar stimulus features tend to be clustered. In these cortices, recurrent circuitry is primarily local and serves to connect cells with similar receptive fields (Braitenberg and Schüz, 1998; Ko et al., 2011). As a consequence, this circuitry is thought to increase signal-to-noise (Douglas et al., 1995) and sharpen the tuning of neurons to specific features of the stimulus (Anderson et al., 2000; Murphy and Miller, 2009; Wehr and Zador, 2003; Wilent and Contreras, 2005). Longer-range parasagittal connections in neocortex are specific and connect areas that respond to similar features (Gilbert, 1992). In piriform cortex, pyramidal cells receive random, convergent input from multiple glomeruli,

NIH-PA Author Manuscript

NIH-PA Author Manuscript

NIH-PA Author Manuscript

and an odor activates an ensemble of neurons distributed across the cortex. Recurrent projections in piriform are long-range, span the entire cortex, and exhibit no apparent topography. This extensive recurrent circuitry may therefore enable an ensemble of active piriform neurons to function as a highly associative, homogenous network.

Experimental Procedures

All experiments followed approved national and institutional guidelines of the Columbia University Medical Center. Methods and materials are described in detail in Supplemental Experimental Procedures.

Animals and virus injection

Lentivirus expressed *Cre Recombinase-GFP* under control of a human Synapsin promoter. AAV2/1 was produced from the vector, pAAV-EF1a-DIO-hChR2(H134R)-EYFP-WPRE-pA plasmid (gift from Karl Deisseroth). Young adult C57/BL6 mice (4–8 weeks old) were anaesthetized with ketamine/xylazine and placed in a stereotaxic device. Individual aliquots of lentivirus and AAV were thawed, mixed (1:1), and injected into anterior piriform cortex through a glass pipette (681 ± 64 nl, range 200–1250 nl) using standard procedures (Cetin et al., 2006).

Electrophysiology and Analysis

Eighteen ± 1 days (range 13–28) after virus injection, mice were anesthetized with isofluorane and decapitated. Parasagittal brain slices (300 μm) were cut using a vibrating microtome (Leica). Experiments were performed using a Cs-gluconate-based intracellular solution for voltage-clamp experiments or a K-methylsulfonate-based intracellular solution for current clamp experiments. All intracellular solutions contained AlexaFluor 594 cadaverine and biocytin to confirm that we only recorded from layer II pyramidal cells. Short, collimated light pulses from a 470 nm LED (LEDC5, Thor Labs) were delivered to the tissue through the objective (40×, N.A. 0.8) every 10–15 seconds. Data were collected and analyzed off-line using AxographX and IGOR Pro (Wavemetrics). All experiments were done at 34°C. Traces typically represent averages of 6–10 trials. Unless stated otherwise, data are presented as mean ± s.e.m.

Histology and imaging

Animals were anesthetized and perfused with cold PBS followed by 4% paraformaldehyde, and postfixed overnight. Coronal sections (100 μm) were cut on a vibrating microtome. Slices were incubated in chicken anti-GFP and rabbit anti-Cre antibodies, and counter-stained with NeuroTrace 640. For visualizing patched neurons, slices were incubated in a rabbit anti-GFP antibody and Streptavidin, AlexaFluor 555 conjugate and counter-stained with NeuroTrace 640. Slices were imaged with a Zeiss 710 confocal microscope.

Supplementary Material

Refer to Web version on PubMed Central for supplementary material.

Acknowledgments

We thank Karl Deisseroth and Ed Callaway for generously providing reagents and P. Kisloff for assistance with manuscript preparation. This work was supported by The Robert Leet and Clara Guthrie Patterson Trust and a National Institute on Deafness and Other Communication Disorders (NIDCD) K99 grant (K.M.F.), a Ruth L. Kirschstein National Research Service Award predoctoral fellowship from the National Institutes of Health (D.L.S.), the Howard Hughes Medical Institute (S.A.S. and R.A.) and a grant from the Mathers Foundation (R.A.).

NIH-PA Author Manuscript

NIH-PA Author Manuscript

NIH-PA Author Manuscript

References

Anderson JS, Carandini M, Ferster D. Orientation tuning of input conductance, excitation, and inhibition in cat primary visual cortex. J Neurophysiol. 2000; 84:909–926. [PubMed: 10938316]

Barkai E, Bergman RE, Horwitz G, Hasselmo ME. Modulation of associative memory function in a biophysical simulation of rat piriform cortex. J Neurophysiol. 1994; 72:659–677. [PubMed: 7527075]

Bathellier B, Margrie TW, Larkum ME. Properties of piriform cortex pyramidal cell dendrites: implications for olfactory circuit design. J Neurosci. 2009; 29:12641–12652. [PubMed: 19812339]

Boyden ES, Zhang F, Bamberg E, Nagel G, Deisseroth K. Millisecond-timescale, genetically targeted optical control of neural activity. Nature Neuroscience. 2005; 8:1263–1268.

Bozza T, McGann JP, Mombaerts P, Wachowiak M. In vivo imaging of neuronal activity by targeted expression of a genetically encoded probe in the mouse. Neuron. 2004; 42:9–21. [PubMed: 15066261]

Braitenberg, V.; Schüz, A. Cortex: Statistics and Geometry of Neuronal Connectivity. Springer-Verlag; Heidelberg: 1998.

Buck L, Axel R. A novel multigene family may encode odorant receptors - a molecular basis for odor recognition. Cell. 1991; 65:175–187. [PubMed: 1840504]

Cang J, Isaacson JS. In vivo whole-cell recording of odor-evoked synaptic transmission in the rat olfactory bulb. J Neurosci. 2003; 23:4108–4116. [PubMed: 12764098]

Cetin A, Komai S, Eliava M, Seeburg PH, Osten P. Stereotaxic gene delivery in the rodent brain. Nature Protocols. 2006; 1:3166–3173.

Chess A, Simon I, Cedar H, Axel R. Allelic inactivation regulates olfactory receptor gene expression. Cell. 1994; 78:823–834. [PubMed: 8087849]

Datiche F, Litaudon P, Cattarelli M. Intrinsic association fiber system of the piriform cortex: a quantitative study based on a cholera toxin B subunit tracing in the rat. J Comp Neurol. 1996; 376:265–277. [PubMed: 8951642]

Davison IG, Ehlers MD. Neural Circuit Mechanisms for Pattern Detection and Feature Combination in Olfactory Cortex. Neuron. 2011; 70:82–94. [PubMed: 21482358]

Dodge FA Jr. Miledi R, Rahamimoff R. Strontium and quantal release of transmitter at the neuromuscular junction. J Physiol. 1969; 200:267–283. [PubMed: 4387376]

Douglas RJ, Koch C, Mahowald M, Martin KA, Suarez HH. Recurrent excitation in neocortical circuits. Science. 1995; 269:981–985. [PubMed: 7638624]

Franks KM, Isaacson JS. Synapse-specific downregulation of NMDA receptors by early experience: A critical period for plasticity of sensory input to olfactory cortex. Neuron. 2005; 47:101–114. [PubMed: 15996551]

Franks KM, Isaacson JS. Strong single-fiber sensory inputs to olfactory cortex: Implications for olfactory coding. Neuron. 2006; 49:357–363. [PubMed: 16446140]

Ghosh S, Larson SD, Hefzi H, Marnoy Z, Cutforth T, Dokka K, Baldwin KK. Sensory maps in the olfactory cortex defined by long-range viral tracing of single neurons. Nature. 2011; 472:217–220. [PubMed: 21451523]

Gilbert CD. Horizontal integration and cortical dynamics. Neuron. 1992; 9:1–13. [PubMed: 1632964]

Goda Y, Stevens CF. Two components of transmitter release at a central synapse. Proc Natl Acad Sci U S A. 1994; 91:12942–12946. [PubMed: 7809151]

Haberly LB. Parallel-distributed processing in olfactory cortex: new insights from morphological and physiological analysis of neuronal circuitry. Chem Senses. 2001; 26:551–576. [PubMed: 11418502]

Haberly LB, Bower JM. Olfactory cortex: model circuit for study of associative memory? Trends Neurosci. 1989; 12:258–264. [PubMed: 2475938]

Haberly LB, Price JL. Association and commissural fiber systems of olfactory cortex of rat. 1. Systems originating in piriform cortex and adjacent areas. Journal of Comparative Neurology. 1978; 178:711–740. [PubMed: 632378]

NIH-PA Author Manuscript

NIH-PA Author Manuscript

NIH-PA Author Manuscript

Johnson DM, Illig KR, Behan M, Haberly LB. New features of connectivity in piriform cortex visualized by intracellular injection of pyramidal cells suggest that “primary” olfactory cortex functions like “association” cortex in other sensory systems. J Neurosci. 2000a; 20:6974–6982. [PubMed: 10995842]

Johnson DMG, Illig KR, Behan M, Haberly LB. New features of connectivity in piriform cortex visualized by intracellular injection of pyramidal cells suggest that “primary” olfactory cortex functions like “association” cortex in other sensory systems. Journal of Neuroscience. 2000b; 20:6974–6982. [PubMed: 10995842]

Ketchum KL, Haberly LB. Membrane currents evoked by afferent fiber stimulation in rat piriform cortex. 1. Current source-density analysis. Journal of Neurophysiology. 1993; 69:248–260. [PubMed: 8381858]

Ko H, Hofer SB, Pichler B, Buchanan KA, Sjostrom PJ, Mrsic-Flogel TD. Functional specificity of local synaptic connections in neocortical networks. Nature. 2011; 473:87–91. [PubMed: 21478872]

Linster C, Hasselmo ME. Neuromodulation and the functional dynamics of piriform cortex. Chem Senses. 2001; 26:585–594. [PubMed: 11418504]

Luna VM, Schoppa NE. GABAergic circuits control input-spike coupling in the piriform cortex. Journal of Neuroscience. 2008; 28:8851–8859. [PubMed: 18753387]

Luskin MB, Price JL. The laminar distribution of intracortical fibers originating in the olfactory cortex of the rat. Journal of Comparative Neurology. 1983a; 216:292–302. [PubMed: 6863605]

Luskin MB, Price JL. The topographic organization of associational fibers of the olfactory system in the rat, including centrifugal fibers to the olfactory bulb. Journal of Comparative Neurology. 1983b; 216:264–291. [PubMed: 6306065]

Malnic B, Hirono J, Sato T, Buck LB. Combinatorial receptor codes for odors. Cell. 1999; 96:713–723. [PubMed: 10089886]

Margrie TW, Schaefer AT. Theta oscillation coupled spike latencies yield computational vigour in a mammalian sensory system. J Physiol. 2003; 546:363–374. [PubMed: 12527724]

McGinley MJ, Westbrook GL. Membrane and synaptic properties of pyramidal neurons in the anterior olfactory nucleus. J Neurophysiol. 2011; 105:1444–1453. [PubMed: 21123663]

Meister M, Bonhoeffer T. Tuning and topography in an odor map on the rat olfactory bulb. J Neurosci. 2001; 21:1351–1360. [PubMed: 11160406]

Miyamichi K, Amat F, Moussavi F, Wang C, Wickersham I, Wall NR, Taniguchi H, Tasic B, Huang ZJ, He ZG, et al. Cortical representations of olfactory input by trans-synaptic tracing. Nature. 2011; 472:191–196. [PubMed: 21179085]

Mombaerts P, Wang F, Dulac C, Chao SK, Nemes A, Mendelsohn M, Edmondson J, Axel R. Visualizing an olfactory sensory map. Cell. 1996; 87:675–686. [PubMed: 8929536]

Murphy BK, Miller KD. Balanced amplification: a new mechanism of selective amplification of neural activity patterns. Neuron. 2009; 61:635–648. [PubMed: 19249282]

Nagel G, Szellas T, Huhn W, Kateriya S, Adeishvili N, Berthold P, Ollig D, Hegemann P, Bamberg E. Channelrhodopsin-2, a directly light-gated cation-selective membrane channel. Proc Natl Acad Sci U S A. 2003; 100:13940–13945. [PubMed: 14615590]

Neville, KR.; Haberly, LB. Olfactory Cortex. In: Shepherd, GM., editor. The Synaptic Organization of the Brain. Oxford; New York: 2004.

Petreanu L, Mao T, Sternson SM, Svoboda K. The subcellular organization of neocortical excitatory connections. Nature. 2009; 457:1142–1145. [PubMed: 19151697]

Poo C, Isaacson JS. Odor Representations in Olfactory Cortex: “Sparse” Coding, Global Inhibition, and Oscillations. Neuron. 2009; 62:850–861. [PubMed: 19555653]

Poo C, Isaacson JS. A major role ofor intracortical circuits in the strength and tuning of odor-evoked excitation in olfactory cortex. Neuron. 2011 in press.

Price JL. An autoradiographic study of complementary laminar patterns of termination of afferent fibers to the olfactory cortex. J Comp Neurol. 1973; 150:87–108. [PubMed: 4722147]

Rubin BD, Katz LC. Optical imaging of odorant representations in the mammalian olfactory bulb. Neuron. 1999; 23:499–511. [PubMed: 10433262]

NIH-PA Author Manuscript

NIH-PA Author Manuscript

NIH-PA Author Manuscript

Saar D, Grossman Y, Barkai E. Learning-induced enhancement of postsynaptic potentials in pyramidal neurons. J Neurophysiol. 2002; 87:2358–2363. [PubMed: 11976373]

Schikorski T, Stevens CF. Quantitative fine-structural analysis of olfactory cortical synapses. Proc Natl Acad Sci U S A. 1999; 96:4107–4112. [PubMed: 10097171]

Sosulski DL, Bloom ML, Cutforth T, Axel R, Datta SR. Distinct representations of olfactory information in different cortical centres. Nature. 2011; 472:213–216. [PubMed: 21451525]

Stettler DD, Axel R. Representations of Odor in the Piriform Cortex. Neuron. 2009; 63:854–864. [PubMed: 19778513]

Stevens CF. Structure of cat frontal olfactory cortex. J Neurophysiol. 1969; 32:184–192. [PubMed: 5775140]

Stokes CCA, Isaacson JS. From Dendrite to Soma: Dynamic Routing of Inhibition by Complementary Interneuron Microcircuits in Olfactory Cortex. Neuron. 2010; 67:452–465. [PubMed: 20696382]

Suzuki N, Bekkers JM. Distinctive Classes of GABAergic Interneurons Provide Layer-Specific Phasic Inhibition in the Anterior Piriform Cortex. Cerebral Cortex. 2010; 20:2971–2984. [PubMed: 20457693]

Suzuki N, Bekkers JM. Two layers of synaptic processing by principal neurons in piriform cortex. J Neurosci. 2011; 31:2156–2166. [PubMed: 21307252]

Uchida N, Takahashi YK, Tanifuji M, Mori K. Odor maps in the mammalian olfactory bulb: domain organization and odorant structural features. Nat Neurosci. 2000; 3:1035–1043. [PubMed: 11017177]

Wehr M, Zador AM. Balanced inhibition underlies tuning and sharpens spike timing in auditory cortex. Nature. 2003; 426:442–446. [PubMed: 14647382]

Wickersham IR, Finke S, Conzelmann KK, Callaway EM. Retrograde neuronal tracing with a deletion-mutant rabies virus. Nat Methods. 2007; 4:47–49. [PubMed: 17179932]

Wilent WB, Contreras D. Dynamics of excitation and inhibition underlying stimulus selectivity in rat somatosensory cortex. Nat Neurosci. 2005; 8:1364–1370. [PubMed: 16158064]

Wilson DA, Stevenson RJ. The fundamental role of memory in olfactory perception. Trends Neurosci. 2003; 26:243–247. [PubMed: 12744840]

Wilson M, Bower JM. Cortical oscillations and temporal interactions in a computer simulation of piriform cortex. J Neurophysiol. 1992; 67:981–995. [PubMed: 1316954]

NIH-PA Author Manuscript

NIH-PA Author Manuscript

NIH-PA Author Manuscript

Highlights

- Recurrent connections extend, undiminished, across millimeters of piriform cortex.
- Despite low connectivity rates, total recurrent input may exceed bulbar input.
- Global excitation is coupled to strong, local feedback inhibition.
- The recurrent network can dynamically alter the response to bulbar input.

NIH-PA Author Manuscript

NIH-PA Author Manuscript

NIH-PA Author Manuscript

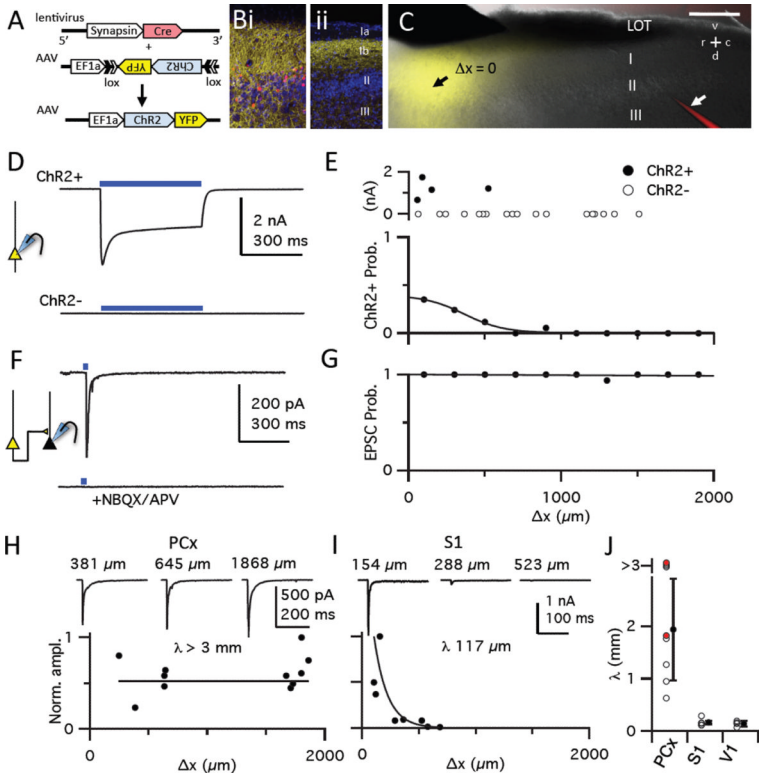

Figure 1. Recurrent excitatory synapses extend undiminished across piriform cortex

(A) Strategy for robust but sparse ChR2 expression. High-titer AAV, used to express Cre-dependent ChR2-EYFP under the control of the strong, ubiquitous EF1α promoter was co-injected with lentivirus encoding Cre recombinase driven by the human synapsin 1 promoter. (B) Confocal images of a virally infected slice. At the injection site (i), membrane-localized ChR2-YFP (yellow) and Cre (red) expression are observed in the cell body layer (II/lII) and dense axonal projections are seen in layers Ib and III. At a site 1 mm caudal to the injection site (ii), only ChR2-labelled axons are seen in layer Ib and III. (C) Focal ChR2-YFP expression in layer II/III neurons in an acute brain slice. The point in layer II at which YFP fluorescence was maximal was defined as the center of the infected area (Δx = 0, black arrow). Cells were visualized with AlexaFluor 594 cadaverine in the patch pipette (bottom right, white arrow). Bulbar inputs were activated by a concentric bipolar stimulating electrode in the LOT (top left). Scale bar, 500 μm. (D) 500 ms light pulses (blue bars) evoked large, sustained photocurrents in some cells. These two cells were <50 μm apart. These recordings were obtained in the presence of NBQX, APV, GBZ, TTX and 4-AP to isolate photocurrents. (E) Top: Size of sustained photo-activated currents from 22 cells from one slice as a function of distance from site of infection (200 μm bins; see G for x-axis scale). $ChR2^+$ cells defined by the presence of sustained photocurrents >10 pA. Bottom: Probability of recording from a $ChR2^+$ cell as function of distance, fit by a normal distribution (width ± S.D.: 368 μm ± 20.2 μm; n=166 cells from 11 slices). (F) Voltage clamp recording from a $ChR2^-$ neuron far from site of infection (Δx, 1250 μm) showing current at −70 mV following a 2 ms light pulse in absence (top) or presence (bottom) of NBQX/APV. (G) Fraction of $ChR2^-$ neurons exhibiting a light-evoked EPSC as a function of distance from the site of infection. Solid line, linear fit. (H) Normalized EPSC amplitudes from 11 cells recorded at different Δx in one piriform slice. Representative traces recorded at different Δx are shown above. EPSC amplitudes from all cells (≥ 5 cells/slice) were scaled to the largest response, and an exponential fit with a length constant (λ) was forced to the data, with an imposed ceiling of λ = 3 mm. (I) Same as H for S1 cortex. (J) Summary of

λs. Open circles, λs for each slice; red circles, λs measured in TTX/4-AP; black circles, mean ± S.D.; piriform, 2.04 ± 0.97 mm, n=8; S1, 0.255 ± 0.226 mm, n=5; V1, 0.144 ± 0.052 mm; n=4.

NIH-PA Author Manuscript
NIH-PA Author Manuscript
NIH-PA Author Manuscript

NIH-PA Author Manuscript

NIH-PA Author Manuscript

NIH-PA Author Manuscript

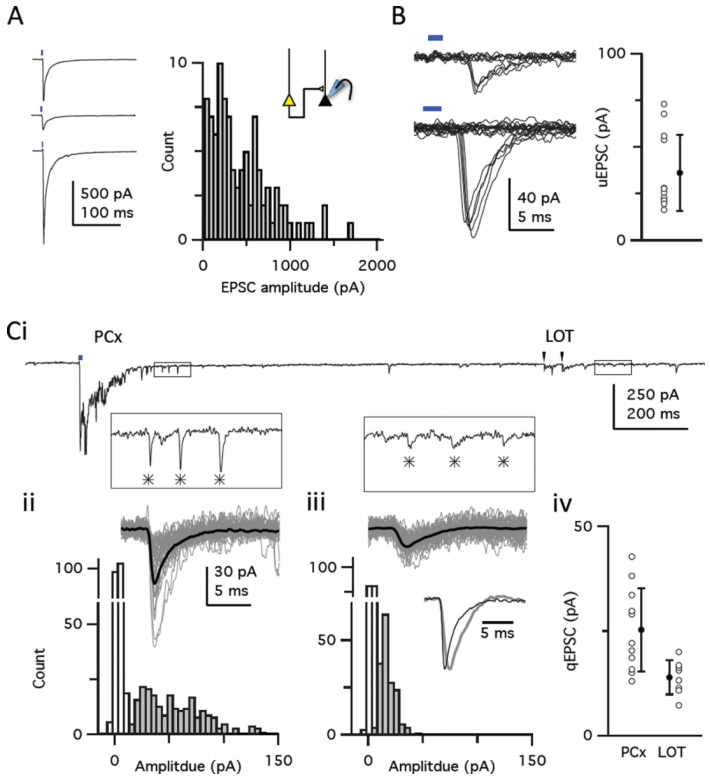

Figure 2. Recurrent excitatory piriform synapses are sparse and weak

(A) Variability of light-evoked EPSC amplitudes at sites far from viral infection. Left: Sequential recording from three cells; Δx: top, 910 μm; middle, 702 μm; bottom, 692 μm. Right: Distribution of light-evoked EPSC amplitudes recorded from 95 cells in 11 slices (one slice per animal). (B) Light-evoked uEPSCs recorded at −70 mV in ChR2^{-} layer II pyramidal cells. Left: Examples of responses and failures from two cells that were evoked with low intensity, focal light pulses distant to the recorded cell (range: 245–408 μm), showing `all-or-none' responses presumably caused by threshold firing of single ChR2^{+} axonal inputs. Right: Individual uEPSC amplitudes (open circles) and average uEPSC amplitude ± S.D. (filled circle) (Ci) Quantal EPSCs (qEPSCs) evoked by light or LOT stimulation when extracellular Ca^{2+} was replaced with Sr^{2+}. Insets at an expanded scale correspond to boxed regions in the upper trace. indicates qEPSCs. (ii) Top: Fifty individual traces (grey) and ensemble average (black) of quantal events evoked by the light pulse. Bottom: The distribution of qEPSC amplitudes (filled bars) and noise (open bars) in this cell. (iii) Same as ii but for events following electrical stimulation of the LOT. (iv) Mean amplitude of light-evoked (n=11 cells) and LOT-evoked (n=9 cells) qEPSCs for each cell (open circles) and for the population (filled circles). Bars show S.D.

NIH-PA Author Manuscript

NIH-PA Author Manuscript

NIH-PA Author Manuscript

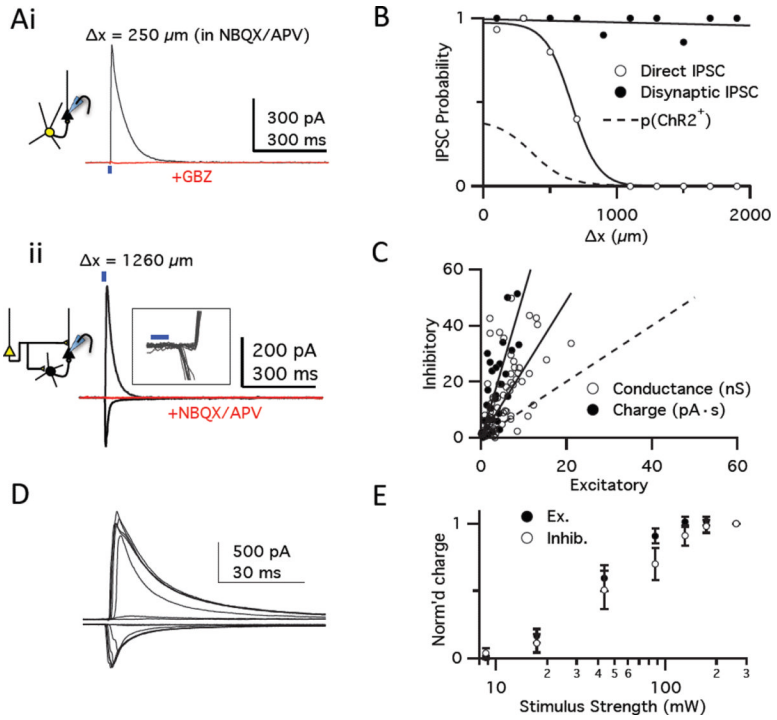

Figure 3. Recurrent excitation drives local strong, scaled inhibition

(Ai) A light-activated IPSC recorded at +5 mV from a ChR2^{-} layer II pyramidal cell near the site of infection (Δx, 250 μm). Responses in NBQX/APV were blocked by GBZ (red traces), indicating IPSCs were caused by direct inhibitory inputs from ChR2^{+} GABAergic interneurons. Blue bar, 2 ms light pulse. (ii) EPSCs (recorded at −70 mV) and IPSCs (recorded at +5 mV) in a pyramidal cell far from site of infection (Δx = 1260 μm). Both responses were blocked by NBQX/APV (overlaid red traces at −70 mV and +5 mV), indicating that these were disynaptic IPSCs evoked by activating excitatory ChR2^{+} axons that, in turn, recruited ChR2^{-} interneurons. Inset: Individual traces at an expanded scale showing that inward EPSCs preceded outward IPSCs. (B) Probability of observing direct (open circles, sigmoid fit) or disynaptic (filled circles, linear fit) IPSCs as a function of distance from site of infection. Dashed line, distribution of ChR2^{+} neurons from 1E. (C) Relationship of excitatory (−70 mV) and disynaptic inhibitory (+5 mV) responses in each cell. Graph shows peak conductance (open circles; slope, 2.45; r = 0.55) and integrated charge transfer (filled circles; 20 ms after light pulses; slope, 5.2 ± 0.53; r = 0.87). Dashed line, relation if inhibitory and excitatory responses were equal. All cells recorded at Δx > 800 μm. (D) EPSCs (top) and disynaptic IPSCs (bottom) evoked in a cell following 2-ms light pulses at different intensities. (E) Summary input/output relationship of excitatory and inhibitory charge transfer (n=11) showing that inhibition scales with excitation. Responses are normalized to those at highest light intensity.

NIH-PA Author Manuscript

NIH-PA Author Manuscript

NIH-PA Author Manuscript

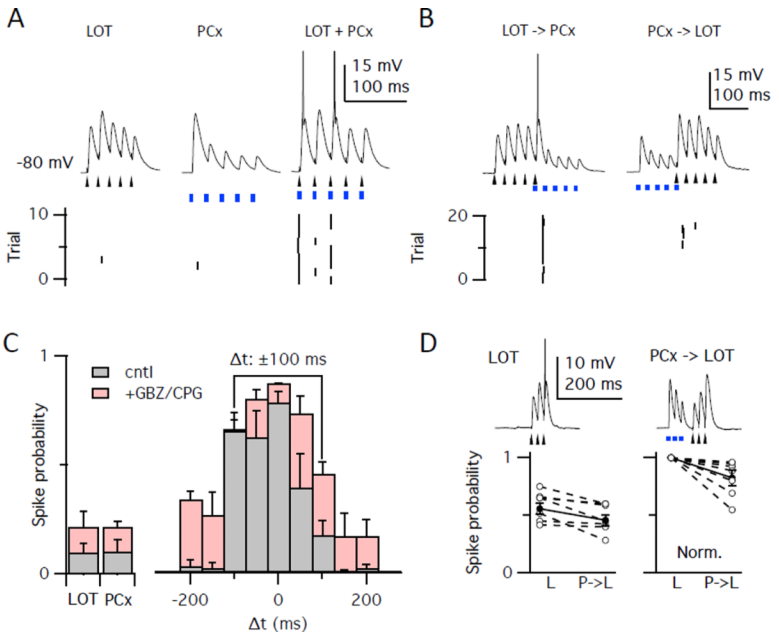

Figure 4. Feedback inhibition shapes piriform activation

(A) Current clamp recordings in a ChR2^{-} pyramidal cell following subthreshold trains (5 pulses at 40 Hz) of electrical stimulation to LOT (arrowheads) to evoke EPSPs from bulbar inputs or light pulses (blue bars) to evoke recurrent PCx inputs. Top: single traces showing synaptic responses with truncated action potentials. Bottom: raster plots of spikes. Stimulus trains were presented alone (left two trains) and simultaneously (right). (B) Left: Presentation of the LOT stimulus train 100 ms before the PCx train. Right: Presentation of the PCx train 100 ms before the LOT stimulus train. (C) Probability of evoking a spike for unpaired LOT and PCX stimuli (left), and with pairing at different intervals (right, Δt = onset of LOT - onset of PCx stimuli). Experiments were performed under control conditions (grey bars, n=6) or with inhibition blocked (red bars, n=4). Line above plot highlights dramatic difference between pairing at Δt = −100 ms versus +100 ms. (D) Strong LOT stimuli evoked spikes on 56% of trials when presented alone, but spiking was suppressed (46%) by preceding, subthreshold PCx stimulation (Δt = 100 ms; n=6). Data show unnormalized (left, paired t-test, p = 0.017) and normalized to unpaired LOT response (right, p=0.022).